communications
earth & environment

ARTICLE

https://doi.org/10.1038/s43247-024-01216-x OPEN

The southward migration of the Antarctic Circumpolar Current enhanced oceanic degassing of carbon dioxide during the last two deglaciations

Xuyuan E. Ai[1,2,11✉], Lena M. Thöle[3,4,5,11✉], Alexandra Auderset[1,10], Mareike Schmitt[1], Simone Moretti[1], Anja S. Studer[1,6], Elisabeth Michel[7], Martin Wegmann[4,8], Alain Mazaud[7], Peter K. Bijl[5], Daniel M. Sigman[2], Alfredo Martínez-García[1✉] & Samuel L. Jaccard[3,4,9✉]

Previous studies suggest that meridional migrations of the Antarctic Circumpolar Current may have altered wind-driven upwelling and carbon dioxide degassing in the Southern Ocean during past climate transitions. Here, we report a quantitative and continuous record of the Antarctic Circumpolar Current latitude over the last glacial-interglacial cycle, using biomarker-based reconstructions of surface layer temperature gradient in the southern Indian Ocean. The results show that the Antarctic Circumpolar Current was more equatorward during the ice ages and shifted ~6° poleward at the end of glacial terminations, consistent with Antarctic Circumpolar Current migration playing a role in glacial-interglacial atmospheric carbon dioxide change. Comparing the temporal evolution of the Antarctic Circumpolar Current mean latitude with other observations provides evidence that Earth's axial tilt affects the strength and latitude range of Southern Ocean wind-driven upwelling, which may explain previously noted deviations in atmospheric carbon dioxide concentration from a simple correlation with Antarctic climate.

[1] Climate Geochemistry Department, Max Planck Institute for Chemistry, Mainz, Germany. [2] Department of Geosciences, Princeton University, Princeton, NJ, USA. [3] Institute of Geological Sciences, University of Bern, Bern, Switzerland. [4] Oeschger Centre for Climate Change Research, University of Bern, Bern, Switzerland. [5] Marine Palynology and Paleoceanography, Department of Earth Sciences, Utrecht University, Utrecht, The Netherlands. [6] Aquatic and Isotope Biogeochemistry, Department of Environmental Sciences, University of Basel, Basel, Switzerland. [7] Laboratoire de Sciences du Climat et de l'Environnement, CEA-CNRS-UVSQ, Université Paris-Saclay, Gif-sur-Yvette, France. [8] Institute of Geography, University of Bern, Bern, Switzerland. [9] Institute of Earth Sciences, University of Lausanne, Lausanne, Switzerland. [10] Present address: School of Ocean and Earth Science, University of Southampton, Southampton, UK. [11] These authors contributed equally: Xuyuan E. Ai, Lena M. Thöle. ✉email: xuyuan.ai@mpic.de; l.m.thole@uu.nl; a.martinez-garcia@mpic.de; samuel.jaccard@unil.ch

On glacial-interglacial timescales, it is believed that the Southern Ocean strongly impacted the atmospheric carbon dioxide (CO_2) inventory owing to its leverage on the communication between the atmosphere and the voluminous ocean carbon reservoir[1,2]. Several mechanisms are proposed to have curbed CO_2 release from the ocean interior during glacial periods, including sea ice expansion[3], an increase in Subantarctic phytoplankton export production fueled by higher iron-bearing dust supply to the surface ocean[4,5], and isolation of Antarctic Zone (AZ) surface waters from CO_2-rich deep water masses[6–12]. Regarding the last mechanism, while several proposals exist for the cause of AZ surface isolation, such as changes in surface buoyancy forcing and changes in abyssal mixing over rough seafloor topography, altered wind-driven upwelling is able to provide a holistic explanation for reconstructed changes in high latitude oceans of both hemispheres, for glacial-interglacial changes as well as millennial-scale events (ref. [9] and references within).

Changes in the position and/or strength of Southern Westerly Winds (SWW) are thought to have modulated Antarctic upwelling[13–15]. Surface winds cause divergent Ekman transport south of the wind stress maximum, near the axis of the Antarctic Circumpolar Current (ACC) between 45°S and 55°S, leading to the upwelling of CO_2- and nutrient-rich subsurface waters along tilted surfaces of constant density. These isopycnals run poleward and upward across the ACC[16], inducing strong meridional gradients in sea surface temperature (SST) and density that define the ACC frontal system[17,18]. The Polar Frontal Zone (PFZ) and the Subantarctic Zone (SAZ), enveloped by the Antarctic Polar Front (APF) to the south and the Subtropical Front (STF) to the north, mark the transition from the cold Antarctic surface water derived from outcropping deep water masses, to the warm Subtropical Zone (STZ) surface waters. The meridional location of this transition has important implications for Southern Ocean overturning circulation and thus the partitioning of CO_2 between ocean and atmosphere and global climate during glacial-interglacial cycles[13,19].

Modern oceanographic data and numerical simulations suggest that the ACC fronts are largely steered by seafloor bathymetry due to the depth structure of the frontal jets, but the extent of frontal shift under substantial climate forcing is still under debate[20,21]. Similarly, model simulations are not consistent in their evaluation of the effect of changing SWW stress on upwelling intensity[22,23]. On glacial-interglacial timescales, available paleoceanographic reconstructions agree on the direction of latitudinal shifts of the ACC fronts[24–29] but do not agree on coherent patterns of change in the SWW[30]. In order to reconstruct changes in Southern Ocean upwelling and identify its drivers, additional quantitative information is needed on the temporal evolution of the ACC fronts on a continuous basis over glacial cycles[9,12,13,19].

To shed light on the timing and structure of Southern Ocean frontal movements and connect these with changes in SWW and upwelling dynamics, we report reconstructions of the meridional gradient in surface layer temperature across the ACC in the southern Indian Ocean based on the TEX^L_{86} paleothermometer, using a revised TEX^L_{86} calibration (Supplementary Note 1). TEX^L_{86} is an organic compound-based proxy that records changes in temperature at the sea surface or the shallow subsurface[31–33] and is thought to be appropriate for polar and subpolar regions (Supplementary Note 2). For simplicity, we refer to both the TEX^L_{86}-reconstructed 0–200 m integrated temperature and World Ocean Atlas (WOA) 2009 0–200 m integrated temperature as sea surface temperature (SST) in this study. We analyze the temporal evolution of reconstructed SST difference (ΔSST) between MD11-3357 (44.68°S, 80.43°E, 3,349 m water depth) and MD11-3353 (50.57°S, 68.39°E, 1568 m water depth) in the Subantarctic and Antarctic zones (SAZ and AZ) of the southeast Indian Ocean, respectively (Fig. 1). The meridional ΔSST between the SAZ and AZ sites is used to investigate the temporal evolution of frontal displacements, based on a simple quantitative framework (see "Methods"). Our focus is the steep temperature gradient in the ACC enveloped by the APF and the STF, so the meridional frontal displacements reconstructed in this study refer to the band of transition from Antarctic surface water to subtropical water rather than a strictly defined front. This approach is enabled by applying the same paleothermometric method to core sites across a large latitudinal range. Our analyses produce a temporally continuous reconstruction of the ACC latitude that lends strong support to the hypothesis of meridional frontal migration during the last glacial cycle, with a generally more equatorward position during cold periods and more

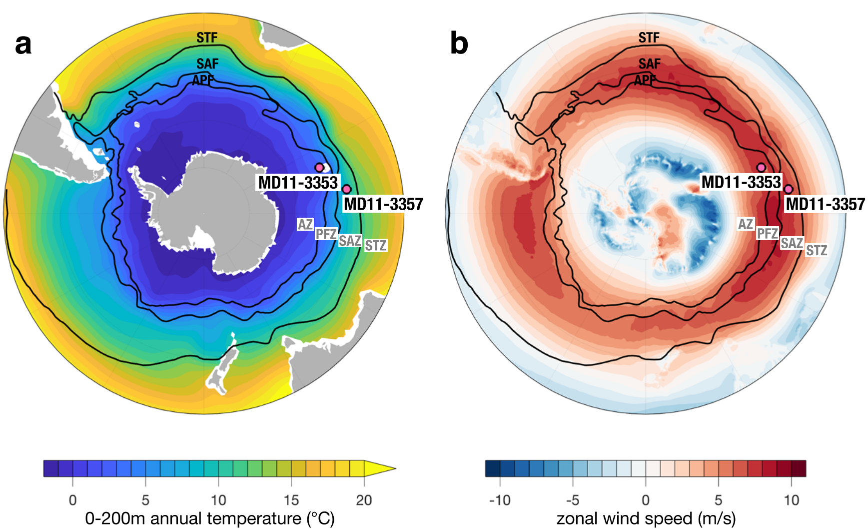

Fig. 1 Maps of modern Southern Ocean 0–200 m annual surface temperature (SST) and 10 m zonal wind. a Annual 0–200 m surface temperature of World Ocean Atlast 2009[45] (°C) and **b** 10 m zonal wind strength based on reanalysis data for the period 1951–1978[78,79]. Pink circles indicate core locations of MD11-3353 (50.57°S, 68.39°E) in the Antarctic Zone (AZ) and MD11-3357 (44.68°S, 80.43°E) in the Subantarctic Zone (SAZ). STF Subtropical Front; SAF Subantarctic Front, APF Antarctic Polar Front, after ref. [18].

poleward location during warm intervals. Based on the results, we argue that the mean position of the SWW had a profound impact on the latitudinal position of the Southern Ocean fronts in the study region. In addition, Earth's axil tilt (obliquity) has been proposed to force changes in atmospheric and oceanic circulation and strongly affects the climate of the middle to high latitude Southern Hemisphere[34]. Asynchrony between CO_2 and Antarctic temperature in late Pleistocene ice core records is found to be associated with obliquity[35], and recent reconstruction of Antarctic Zone surface nutrient conditions has provided evidence for a mechanistic link between obliquity and this asynchrony via its modification of Antarctic upwelling and CO_2 outgassing during the last glacial cycle[12]. The quantitative, temporally continuous reconstruction of the ACC latitude in this work allows identification of the effect of obliquity on ACC isotherms, providing additional support for the effect of obliquity on SWW intensity and Antarctic upwelling.

Results and discussion

Fidelity of TEX^L_{86} in the Kerguelen region. The TEX_{86} paleothermometer is based on the relationship between SST and the distribution of archaeal membrane lipids (glycerol dibiphytanyl glycerol tetraethers [GDGTs])[31]. In polar and subpolar regions, the TEX^L_{86} index has been shown to provide more realistic paleotemperature estimates than the TEX_{86} index[32,33]. The main difference between the two indices is that TEX^L_{86} does not include the crenarchaeol regioisomer, which is found only in low abundances at SSTs below 15 °C (Supplementary Fig. 1)[33]. Numerous studies have applied TEX^L_{86} in the (sub)polar regions for downcore temperature reconstruction[12,32,36–41]. The offset of reconstructed TEX^L_{86}-SST (compared to WOA09 SST) for the global core-top compilation[42] is ±3.2 °C (Supplementary Note 3), which is likely due to influences from factors such as the depth and seasonality of GDGT export, archaeal community change, and terrestrial GDGT input[43], on top of potential interlaboratory variation[44]. Previous studies postulated that in more restricted localities, the error of TEX^L_{86} SST reconstruction is smaller than that in the global TEX^L_{86} calibration, since these factors are less variable within a given region. Within the Indo-Pacific ACC core-tops, although there is a tendency for TEX^L_{86} to overestimate SSTs in this region, our revised TEX^L_{86} calibration accurately captures the SST difference (ΔSST) between any two sites (Supplementary Note 3). This is likely due to a relatively uniform non-thermal contribution to TEX^L_{86} within the region. The offset of reconstructed TEX^L_{86} ΔSST (compared to WOA09 ΔSST) between any two core-tops within a specific region of the ACC is overall smaller than that between any two core-tops in the whole ACC, supporting the hypothesis of more similar non-thermal factors in more restricted oceanographic settings (Supplementary Note 3).

The overall glacial-interglacial change of TEX^L_{86}-SST at the two sites agree well with SST records of other paleothermometry methods from nearby sites (Supplementary Note 4). The youngest (core-top) samples from MD11-3357 and MD11-3353 (with estimated ages of 1.06 ka and 0.79 ka, respectively) provide SST estimates of 12.9 °C and 4.1 °C, respectively (Fig. 2), 3.0 °C and 1.3 °C warmer than the WOA09 SST[45] (9.9 °C and 2.8 °C, respectively). These errors lie within ±1 standard deviation for the Indo-Pacific ACC core-tops (Supplementary Note 3). The GDGT indices related to several non-thermal factors fall within the expected range for the two core sites (Supplementary Note 5), suggesting that the tendency to overestimate SST at the two sites may be due to non-thermal contributions not reflected in these GDGT indices. The TEX^L_{86} core-top ΔSST between the two sites is 8.8 °C, 1.7 °C higher than the WOA09 ΔSST. Apart from non-thermal factors mentioned above, this difference between reconstructed core-top ΔSST and modern ΔSST may derive from high frequency SST changes in the Southern Ocean. Millennial-scale SST oscillations of as much as 4 °C have been observed around the Antarctic Peninsula[46], which were synchronous with SST oscillations of ~1 °C in the southwest Pacific in the late Holocene[47]. Given that the surface sediments in the Kerguelen region are often more than one thousand years old[12], an offset of 1.7 °C between the core-top TEX^L_{86} ΔSST and WOA09 ΔSST is reasonable. As MD11-3353 and MD11-3357 are close to each other in the Kerguelen region, the factors potentially affecting TEX^L_{86} temperature reconstruction are likely similar at the two sites throughout the time period of interest. If so, the resulting uncertainties in absolute temperature estimation should be of similar amplitude and of the same direction, such that they should not greatly bias the calculated temperature difference between the two sites. We take 1 °C to be the uncertainty of the reconstructed ΔSST, taking both analytical precision and non-thermal archaeal factors into consideration (Supplementary Note 6).

SST changes and the link to frontal shifts. SSTs at both MD11-3353 and MD11-3357 are closely correlated with Antarctic ice core-reconstructed air temperature[48] (Fig. 2). The records depict a glacial-interglacial SST amplitude of about 9 °C (Fig. 2), in good agreement with multi-proxy SST reconstructions in the area[49,50]. In WOA09, the steepest slope of longitudinally averaged SST in the Kerguelen region lies north of AZ site MD11-3353 and around three-fifths south of SAZ site MD11-3357 (Supplementary Fig. 15). ΔSST would decrease (SSTs would become more similar) if, as a consequence of frontal shifts, both sites recorded temperatures from more similar water masses. This would occur if the fronts shifted either northward or southward.

The reconstructed ΔSST between the two core sites during the past 150 ka shows a pattern distinct from that of the glacial-interglacial climate evolution (Fig. 2a). This pattern is not a result of uncertainties in the age model (Supplementary Note 7). During peak glacial intervals such as Marine Isotope Stage (MIS) 2, 4, and 6, ΔSST is reduced to 4.5–6 °C. It reaches maximum values of >7.5 °C during intermediate climate intervals, such as MIS 5c and MIS 3, while during peak interglacials, ΔSST drops again to 4–6 °C. A cross-plot between ΔSST and the Antarctic ice-core (EPICA Dome C (EDC)) temperature reconstruction supports the inference that ΔSST decreases as climate approaches peak cold and warm climate states and reaches highest values under intermediate climate conditions (Fig. 3a). This non-monotonic relationship between ΔSST and EDC temperature suggests that the ACC fronts have shifted northward and southward as climate changed.

To understand the impact of frontal shifts on ΔSST between the selected core sites, we use a simple quantitative framework to illustrate the responses of SST at individual sites and ΔSST between sites to latitudinal migrations of the ACC and explore the outputs of different scenarios of coupling between frontal latitude and regional climate under different setups of the framework (Fig. 3; see "Methods", Supplementary Note 8 & 9). We first simplified the meridional SST profile in the Kerguelen region in WOA09 into three segments, the AZ segment, the Polar Transition Zone (PTZ) segment—which includes the PFZ and SAZ—and the STZ segment, respectively. Then we applied different parameters to alter the three segments, mimicking hypothetical frontal changes, while assuming that the width of the PTZ has been constant. The parameters dictating the response of ΔSST to a certain ACC latitude change in this quantitative framework are the ranges of glacial-interglacial SST change in the AZ and the STZ, respectively, which reflect the extent of polar amplification. For the sensitivity analysis, we explored the changes of ΔSST between our sites compared to Antarctic climate (with EDC temperature taken as representing the latter) under different scenarios of coupling between frontal latitude and

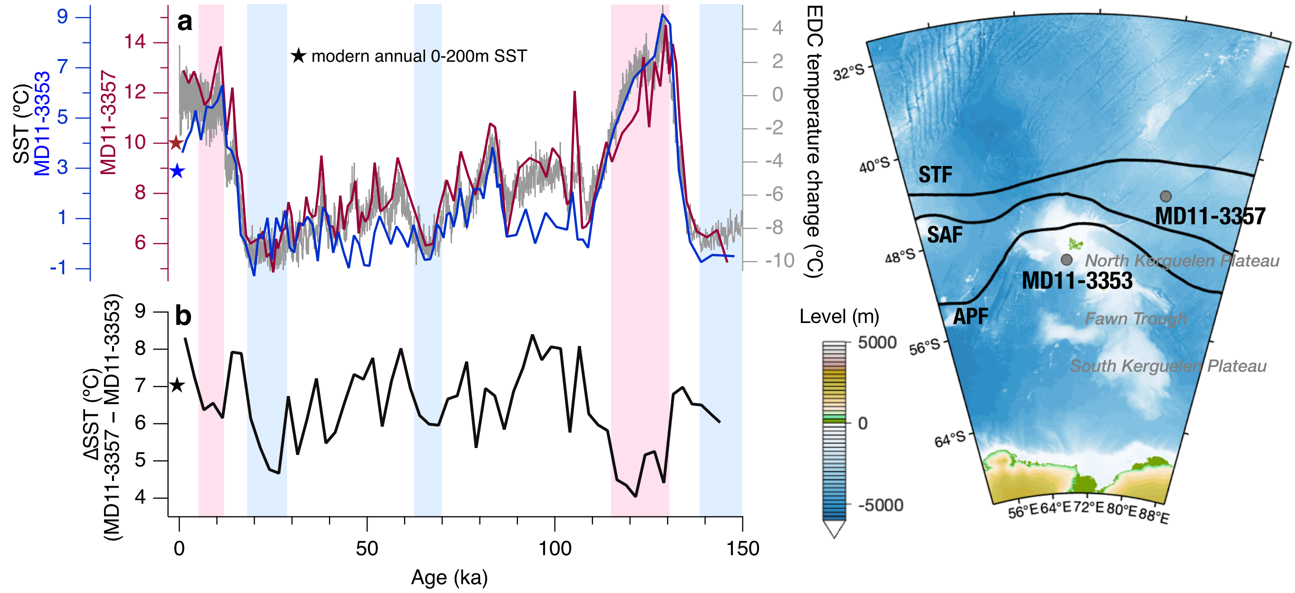

Fig. 2 Sea surface temperature (SST) reconstructions across the last glacial cycle. a GDGT-based (TEX^L_{86}) SST reconstruction for core MD11-3357 (red) and core MD11-3353 (blue), compared to the EPICA Dome C (EDC) temperature change[48] (gray). **b** SST difference (ΔSST) between the two cores, SST(MD11-3357) − SST(MD11-3353), interpolated on a 2.5 kyr time step. Blue bars indicate cold periods of MIS 2, 4, and 6 and pink bars indicate warm periods of MIS 5e and the early Holocene. Arrows on the y-axis indicate modern annual temperatures of the shallow subsurface (0–200 m)[45]. The map shows the location of the core sites with bathymetry in the Kerguelen region[80]. STF Subtropical Front, SAF Subantarctic Front, APF Antarctic Polar Front, after ref. [18].

regional climate and with different prescribed framework parameters (Supplementary Note 8). In this study, we assume that the relationship between the ACC latitude and Antarctic climate remains linear. This assumption is derived from a linear relationship between global mean temperature and SWW latitude observed in GCM simulations[51], overall synchronicity between southern high latitude SST and global mean SST during the last glacial-interglacial cycle[52], and strong coupling between the steep SST gradient in the Southern Ocean (which we used to define the ACC) and surface wind stress in both modern observations[17] and GCM simulations[53]. The results show that the non-monotonic relationship observed between ΔSST and EDC temperature only exists when the fronts shift alongside Antarctic climate change (Fig. 3, Supplementary Note 8). Altering either the prescribed framework parameters, namely the ranges of SST change in the AZ and the STZ, or the rate of frontal migration relative to Antarctic air temperature change alters the shape of the non-monotonic pattern (Supplementary Figs. 16 and 17).

Based on an estimated maximum glacial-interglacial SST change of 6 °C in the AZ and 2.5 °C in the STZ (Supplementary Note 9), an optimization algorithm was applied to find the linear model between ACC frontal latitude and Antarctic air temperature that best fits the TEX^L_{86}-reconstructed ΔSST between MD11-3357 and MD11-3353: $\Delta lat\ (degrees) = \Delta T_{EDC}\ (°C) * 0.58 + 4.20$ (see "Methods", Supplementary Fig. 19). When we swap the maximum SST change in AZ and STZ (i.e., hypothetical tropical amplification), the optimization algorithm produces a very similar slope for the best-fitting linear model, suggesting that this linear relationship between ACC frontal latitude and Antarctic air temperature is robust and largely insensitive to changes in the prescribed parameters of the framework (Supplementary Fig. 19). Changes in the width of the ACC play a minor role in controlling the relationship between the simulated ΔSST of the two sites and Antarctic air temperature (Supplementary Note 10).

When the location of the ACC is kept unchanged, the simulated ΔSST decreases when climate warms (Fig. 3), which is the result of prescribed polar amplification in the framework. This trend qualitatively matches that of the reconstructed ΔSST for the warmer climate intervals, but the simulated change in ΔSST is too small (Fig. 3d). In addition, the no-shift simulation cannot reproduce the low ΔSST characteristic of the coldest conditions. In contrast, when ACC frontal latitude increases linearly with Antarctic air temperature, the observed non-monotonic relationship between TEX^L_{86}-reconstructed ΔSST and EDC temperature is well-captured (Fig. 3e). This simulation also captures many temporal features in the ΔSST change between the two sites (Fig. 3f) as well as in the glacial-interglacial SST changes at individual core sites (Supplementary Fig. 20). TEX^L_{86} SST data from two additional sites located between the latitudes of MD11-3357 and MD11-3353 also agree with the simulated changes in ΔSST under the best-fitting linear model, albeit with greater uncertainty (Supplementary Note 11), indicating that our framework and the frontal shift model are robust for the southeast Indian Ocean. Within the four sites in the Kerguelen region, MD11-3353 and MD11-3357 likely represent the most appropriate pair to evaluate ΔSST for the effect of ACC migration because they are adequately close for frontal displacements to directly affect the ΔSST between the two sites, while being adequately distant that changes in ΔSST are robust against paleothermometric errors. Thus, our discussion of ACC latitude reconstruction focuses on these two sites.

ACC frontal shifts in the southern Indian Ocean over the last glacial cycle. While bottom topography is an important constraint on the path of barotropic deep ACC currents[23,54], large variability of the ACC fronts upstream and downstream of topographic features has been observed to correlate with SWW shifts induced by changes in Southern Annular Modes in the Indian Southern Ocean[55]. In addition, the warming and freshening trend of the Southern Ocean reflects a southward displacement of isopycnals during the past 40 years[21], and the surface hydrographic frontal structure has been observed to shift southward by about 60 km on a circumpolar average from 1992 to 2007[56]. In the Kerguelen region, from 1992 to 2007, the APF

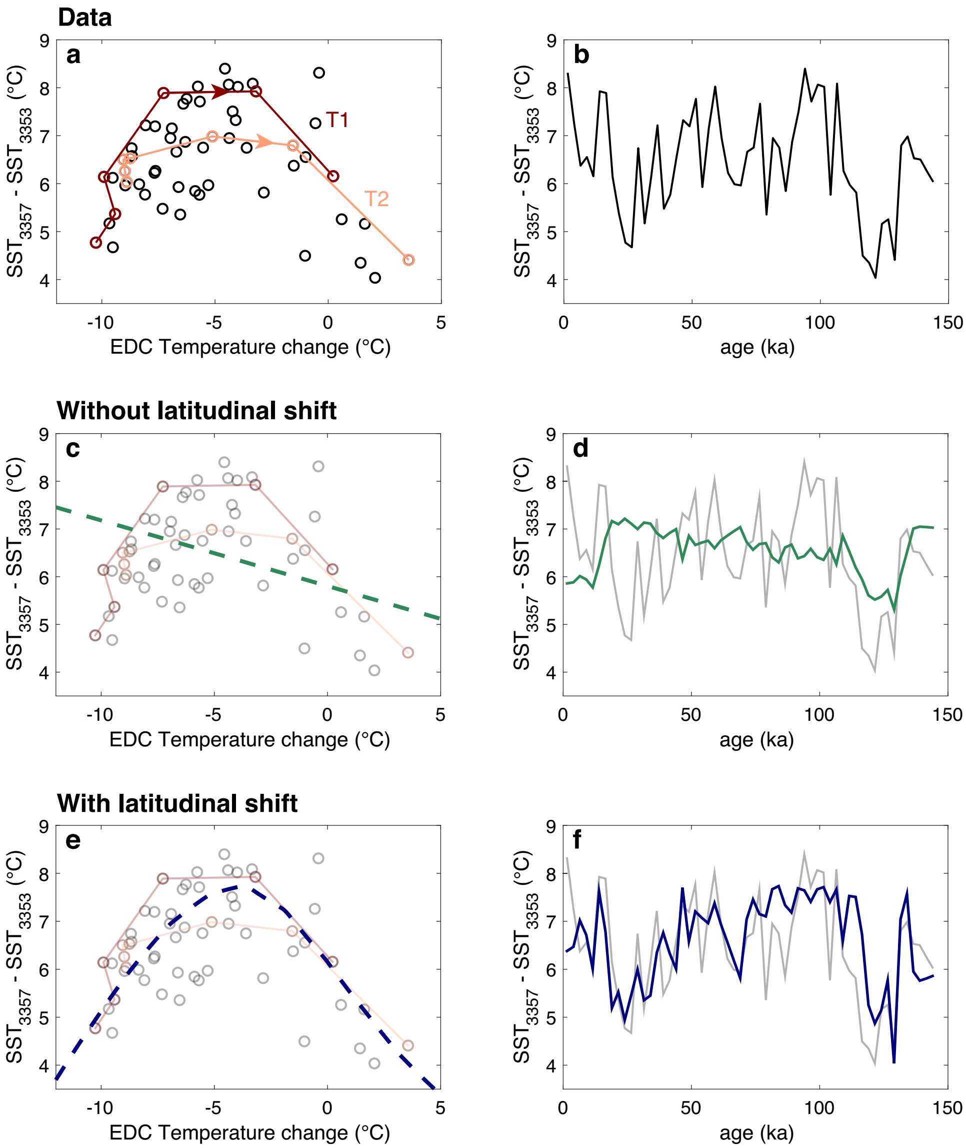

Fig. 3 Data-simulation comparison of the relationship between Antarctic air temperature and the sea surface temperature difference (ΔSST) between the two Southern Ocean sediment cores. a The reconstructed ΔSST in comparison with EPICA Dome C (EDC) temperature depicts a horseshoe pattern with its angular point (largest ΔSST) around −4 °C. Red open circles represent data from the late MIS 2 to the end of Termination 1 (10–24 ka), and the red line and arrow represent the temporal progression of ΔSST towards younger ages. Orange open circles represent data from the late MIS 6 to the end of Termination 2 (129–144 ka), and the orange line and arrow represent the temporal progression of ΔSST towards younger ages. **b** The downcore record of reconstructed ΔSST between MD11-3357 and MD11-3353. **c**, **d** Simulated ΔSST between the latitude of MD11-3357 and that of MD11-3353 without ACC shift (green dashed line and solid line) compared with EDC temperature and age. **e**, **f** Simulated ΔSST with the best-fitting linear model of ACC shift (dark blue dashed line and solid line) compared with EDC temperature and age. The data in (**a**) and (**b**) are plotted semi-transparent in the background of (**c**–**f**).

has been observed to change its position from passing north of the plateau to passing through Fawn Trough[56], suggesting that the ACC fronts can overcome topographic barriers under substantial forcing.

To reconstruct past changes in ACC latitude, using the relationship between ΔSST and ACC latitude inferred from our framework, we include the reconstructed TEX^{L}_{86}-ΔSST between MD11-3353 and MD11-3357 to back-calculate the latitudinal changes of the ACC fronts based on the measured ΔSST (Fig. 4 and Supplementary Fig. 21; see "Methods"). During cold intervals, including MIS 2, MIS 4, and MIS 6, the low ΔSST implies a northward shift of the ACC of ~2° compared to today (Fig. 4d). During the previous interglacial (MIS 5e), SST at MD11-3357 and MD11-3353 were ~2–4 °C warmer compared to pre-industrial, and the reconstructed ΔSST was very low (~4 °C). This suggests that the ACC fronts were as much as 6° further south than today (Fig. 4d), such that the steepest SST gradient moved southward of the AZ core MD11-3353. Our estimated ACC positions for both the LGM and MIS 5e appear to be more poleward than most of frontal shifts estimated in previous studies for the southern Indian Ocean (Supplementary Fig. 24). These studies either assume the same (sub-)isotherm as an ACC front throughout the glacial-interglacial climate change or assume the shift in abundance or size of specific plankton species to be associated with an ACC front. Factors such as homogenous cooling of the deep ocean, response of plankton to glacial-interglacial biogeochemical changes, and season-specific signals may bring uncertainty to frontal shifts based on the above assumptions, explaining the discrepancy in reconstructed frontal shifts between our study and previous studies (Supplementary

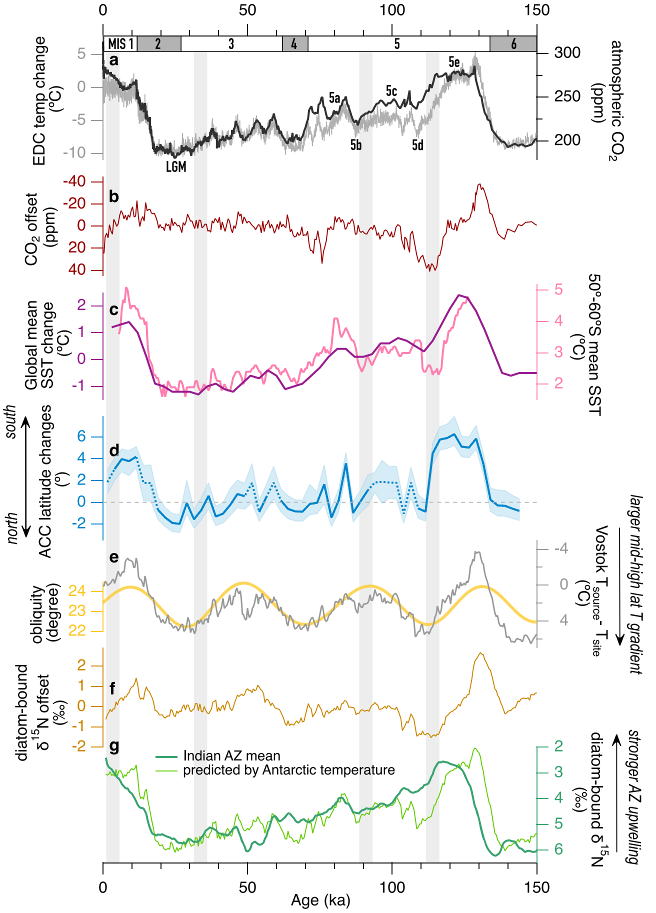

Fig. 4 Meridional migrations of the ACC over the last glacial cycle and their connections to climate and CO_2 change. **a** Atmospheric CO_2[72] (black) and EPICA Dome C (EDC) temperature change[48] (gray). **b** Offset between CO_2 and predicted CO_2 based on a linear relationship between Antarctic ice core temperature and CO_2[12] (dark red). **c** Compilation of SST at 50°–60°S[52] (pink) and global SST change[66] (purple). **d** Changes in ACC latitude calculated from ΔSST (3357−3353) (thick blue solid and dashed lines) and the uncertainty envelope (lighter shading). The dashed line represents where the measured ΔSST corresponds to an uncertainty range of ACC latitude change and the ACC latitude change is estimated as the average of the upper bound and lower bound (see "Methods"). **e** Changes in the difference between air temperatures at the moisture source (T_{source}) and ice core site (T_{site}) of Vostok (dark gray) relative to modern conditions reconstructed from ice deuterium excess[73], and obliquity[81] (yellow). **f** Offset between Indian AZ diatom-bound $\delta^{15}N$ and predicted diatom-bound $\delta^{15}N$ based on a linear relationship between Antarctic air temperature and diatom-bound $\delta^{15}N$[12] (brown), **g** Combined record of Indian AZ diatom-bound $\delta^{15}N$ as an indicator of upwelling[12] (dark green) and predicted diatom-bound $\delta^{15}N$ based on a linear relationship between Antarctic air temperature and diatom-bound $\delta^{15}N$[12]. The numbers at the top indicate Marine Isotope Stages. The vertical gray bars indicate different cooling periods of low obliquity (111.5–116.5 ka in MIS 5d) or lowering obliquity (1.5–6.5 ka in the late Holocene) during warmer conditions, low obliquity during glacial conditions (31.5–36.5 ka in MIS 3), and high obliquity during intermediate conditions (89–94 ka in MIS 5b).

Note 12). The very southward ACC position during MIS 5e reconstructed by our framework is further consistent with the unusually low biogenic opal flux at MD11-3353 during this interval[41], which may be related to silicic acid limitation on diatom growth as a consequence of the more southward location of the APF (Supplementary Note 13 and Supplementary Fig. 25).

According to our framework, the rising temperatures at MD11-3357 and MD11-3353 during the last two glacial terminations were associated with poleward shifts in the ACC fronts that led to an initial increase followed by a decrease in ΔSST (Figs. 2b and 3a), as the steepest part of the meridional SST profile moved first to a position sandwiched between the two sites and then to a position partially south of both sites (Supplementary Fig. 15). At the end of both terminations, ΔSST progressed to a lower range (Fig. 3a), signaling that the fronts are most poleward at the beginning of interglacials (Fig. 4d). There appears to be an offset between the progressions of ΔSST during the two glacial terminations (Fig. 3a), which suggests that the SST structure within the ACC may be subject to more variations than our framework assumes. Nevertheless, the similar shape of the ΔSST progression when plotted over EDC temperature during the two terminations argues that they experienced similar changes in ACC frontal positions (Figs. 3a and 4d).

At the end of Termination 1 and in the early Holocene, the lower reconstructed ΔSST suggests that the steepest part of the meridional SST profile was partially south of MD11-3353 and the ACC fronts reached as much as ~4° southward of the current position (Fig. 4d). This ACC position agrees with a more southward APF in the Kerguelen region reconstructed previously for this time period[25], and is also consistent with the low opal flux observed at MD11-3353 during the last deglaciation and the early Holocene[41] (Supplementary Note 13 and Supplementary Fig. 25). During the late Holocene, while Antarctic air temperature remained stable, the reconstructed ΔSST increased from ~6.5 °C to ~8 °C (Fig. 2), suggesting a gradual northward shift of the ACC fronts to place a greater portion of the steepest meridional SST transition between MD11-3353 and MD11-3357 (Fig. 4d). A northward ACC shift should correspond to a declining EDC temperature, yet the EDC temperature remained stable during this interval, resulting in a leftward trend that deviates from the linear relationship when the EDC temperature change is plotted over ACC latitude change (Fig. 5a). Here, we explore possible explanations for this deviation.

The location of Kerguelen Plateau in the flow path of the ACC (Fig. 2) may have made the fronts more prone to meander upstream and downstream of the plateau[55]. The modern APF to the west of the Kerguelen Plateau is shown to seasonally meander by as much as 4° because of interaction with local topography[57]. The large meander of the APF path may have caused sporadic changes in the width of the ACC, which may contribute to higher ΔSST between MD11-3357 and MD11-3353. The southern Kerguelen bathymetry (Fig. 2) may also help to explain the Holocene deviation from the relationship between EDC temperature and ACC latitude. Civel-Mazens et al.[25] suggested that during the warmer interglacials such as MIS 5e and MIS 9, the ACC is pushed poleward enough that the APF persistently passes through Fawn Trough, which is ~5° southward of the current APF, while the APF only briefly passed through Fawn Trough at the end of the last deglaciation and returned northward to its path north of the Kerguelen Plateau over the later part of Holocene because of the relatively mild climate. The authors also suggested a similar APF position for MIS 7, which is interpreted to be another more moderate interglacial. These interpretations agree with the idea that the bathymetric thresholds may be persistently surpassed in warmer interglacials such as MIS 5e, whereas during the intermediate interglacials such as the Holocene, this threshold was overcome only temporarily by the APF. Thus, the northward shift of the ACC fronts within the Holocene may be the consequence of a failed attempt to cross the bathymetric threshold.

Another possibility is that Antarctic Ocean surface water temperature is decoupled from EDC temperature during the Holocene. The decrease in summer insolation at 65°N in the last

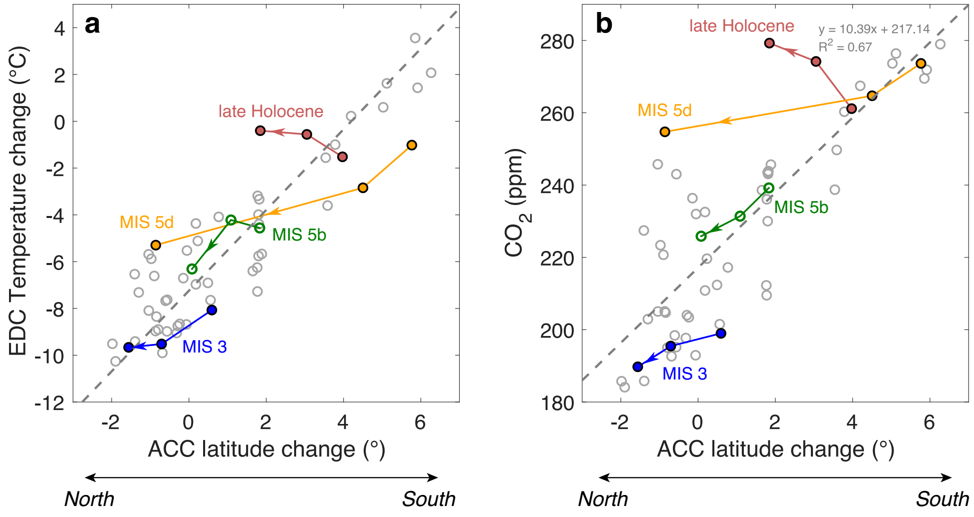

Fig. 5 EDC temperature change and atmospheric CO_2 compared to temporal changes in the latitude range of the ACC. Gray circles represent interpolated **a** EDC temperature changes[48] and **b** CO_2[72] compared to changes in the latitudinal position of the ACC relative to today reconstructed from ΔSST between MD11-3353 and MD11-3357. Gray dashed line in (**a**) represents the best-fitting linear model between EDC temperature and ACC latitude. Gray dashed line in (**b**) represents a linear regression between atmospheric CO_2 and reconstructed ACC latitude change. Filled symbols and lines correspond to the shaded intervals in Fig. 4. Red symbols and arrowed line represent the progression during the late Holocene from 6 ka to 1 ka. Yellow symbols and arrowed line represent the progression during MIS 5d from 116.5 ka to 111.5 ka. Navy symbols and arrowed line represent the progression during MIS 3 from 36.5 ka to 31.5 ka. Open green symbols and arrowed line represent the progression at MIS 5b from 94 ka to 89 ka when obliquity is at maxima. Increased deviation of data from the linear relationship during MIS 2 and MIS 3 in (**a**) may be due to errors in the reconstructed ACC latitude during millennial scale events which are poorly resolved in the TEX^L_{86} SST records. Increased deviation of data from the linear relationship during MIS 2–4 in (**b**) may be due to stronger effects of iron fertilization in the SAZ on CO_2 during these intervals.

10 ka is much smaller compared to that of 115–125 ka, and its cooling effect through the albedo feedback is weak, mostly constrained to the extratropical Northern Hemisphere[58]. The lowering obliquity during the Holocene decreases the insolation received at high latitudes, but it may lead to a relatively weak cooling effect at Antarctica's inland ice core sites, as high albedo would result in little changes in net absorbed radiation. On the other hand, stronger cooling may occur at Antarctica's continental margins and the surrounding Antarctic Ocean. Similar to the TEX^L_{86}-SST at MD11-3353, diatom-based SST records from the AZ in the Indian and Atlantic sector also show a decline during the Holocene[49,59]. SST reconstructions at different sites near the Western Antarctic Peninsula as well as the δD record at Taylor Dome also show cooling temperatures for the last 10 ka, tracking the decline in local insolation[46]. The cooling of the Antarctic Ocean would correspond with a northward shift of the ACC, as predicted by our linear model between Antarctic climate and ACC latitude.

A related explanation, which will be discussed further below, involves the role of obliquity in Southern Ocean upwelling. Declining obliquity over the Holocene is expected to have strengthened the SWW and thus northward Ekman surface water transport and upwelling in the AZ[60,61], consistent with diatom-bound nitrogen isotope reconstructions[12,62] (Fig. 4f, g). Independent of any change in the meridional position of the SWW, this would have pushed surface isotherms equatorward (i.e., increasing the meridional tilt of isopycnals)[63]. Thus, decoupling of ACC frontal position from Antarctic air temperature may be a fingerprint of obliquity-driven changes in upwelling.

Controls on ACC front latitudes. As a result of the back-calculation based on the best-fitting linear model, the temporal evolution of the ACC position deduced from ΔSST is generally correlating with changes in both ice core air temperature[48] and compiled Southern Ocean SSTs[52] (Fig. 4a, c, d). Our results provide quantitative evidence for the connection between Antarctic climate and the position of ACC flow path in the Indian sector of the Southern Ocean over glacial cycles, which allows identification of specific mechanisms that drive changes in the SWW in the Indian sector during climate transitions. ACC shifts during the last glacial cycle reconstructed in the Pacific and Atlantic sector have a similar glacial-interglacial trend as in the Indian sector, but the extents of the shifts appear to be different[26]. It is proposed that in the Pacific Southern Ocean, tropical forcing of the SWW prevails over mid-to-high latitude forcing, suggesting heterogeneity in the changes of the SWW in different Southern Ocean sectors over orbital timescales[64]. Thus, the interpretations of frontal latitude change in the Kerguelen region likely reflect the response of the ACC flow in the Indian Ocean, and the mechanisms identified in the following discussions may not be applicable to other sectors, while this quantitative method opens the door for future investigation of sector-specific ACC dynamics.

Variations in the latitude of SWW and the strong SST gradient that defines the ACC are found to be strongly coupled in modern oceanographic observations[17,53] (Fig. 1). Applying these relationships to frontal shifts in the Indian Southern Ocean over the last glacial cycle, the northward displacements of the ACC during MIS 5d, MIS 4, and MIS 2 argue for coincident northward (equatorward) shifts of the SWW. These intervals are associated with global cooling driven by changes in Earth's orbital parameters, which, according to global climate model simulations, should have driven an equatorward shift of the westerly winds as part of a cooling-driven contraction of the Hadley cell[60,65]. However, the cooling at MIS 5d does not bring global temperature or EDC temperature to LGM levels[48,66], while the coinciding equatorward shift of the ACC does (Fig. 4c, d), which results in an upward trend that slightly deviates from the linear relationship between EDC temperature and ACC latitude (Fig. 5a). Thus, some additional driver is needed to explain the extent of ACC equatorward shift at MIS 5d.

As introduced previously, another important factor in the mid-latitude westerly winds is Earth's obliquity[61]. As a result of the linear correlation between ACC latitude and Antarctic climate and the strong 40 kyr component in the EDC temperature record, the reconstructed ACC latitude over the last glacial cycle partially covaries with the obliquity cycle, with a more northward position associated with low obliquity (Fig. 4d, e). However, obliquity seems to be playing an additional role through its impact on SWW wind intensity, affecting upwelling in the Antarctic Zone and northward transport of cold water. In global climate model simulations, lower obliquity can enhance the mid-latitude temperature gradient, which in turn drives intensification of the mid-latitude westerly winds[60,61,67,68]. In model simulations in which changes in eddy fluxes only partially cancel changes in wind-driven Ekman flow, an increase in wind strength would enhance the residual circulation of the Southern Ocean upper cell and increase the transport of cold water northward, leading to surface cooling to the north of the AZ[63], corresponding with a northward frontal shift. When we compare the progression of EDC temperature with the reconstructed latitudinal migration of the ACC in the Indian Southern Ocean, MIS 5d and the late Holocene, which are characterized by low or declining obliquity, fall to the left of the linear relationship (Fig. 5a), indicating greater northward ACC shift than predicted by EDC temperature change alone. This pattern becomes evident when comparing to MIS 5b, another relatively well-constrained period in our record that is associated with cooling and northward ACC shift but high obliquity, which plots along the linear relationship between EDC temperature and the latitudinal position of the ACC. The difference in the EDC temperature-ACC location relationship between these time intervals suggests that low obliquity can contribute to northward ACC migration by enhancing Antarctic upwelling. Unlike during the late Holocene when the effect of obliquity sustained strong upwelling in the AZ, during MIS 5d, this enhancement in upwelling by obliquity is a secondary effect which is masked by the dominating impact of equatorward ACC shift on the general Southern Ocean overturning circulation that acts to reduce surface-deep exchange. However, similar patterns in the deviation from the observed relationships between EDC temperature and ACC latitude, and between ACC latitude and atmospheric CO_2 during MIS 5d and the late Holocene, point to a uniform link to obliquity, which will be discussed in detail next.

Changes in upwelling and CO_2 outgassing. Changes in the latitude range of the ACC and the SWW may have important consequences for the release of carbon from the deep ocean through its communication with the atmosphere in the Southern Ocean[14]. A northward shift in the SWW would decrease upwelling of deep water in the upper cell of the overturning circulation in the Southern Ocean[13], which would promote carbon storage through a combination of mechanisms[9]. In addition, decreased upwelling of the relatively warmer Circumpolar Deep Water under more equatorward SWW would promote the expansion of quasi-permanent sea ice and shoal the density interface between the lower and upper cells of the Southern Ocean overturning[69], decreasing the deep turbulent mixing and isolate Antarctic Bottom Water from the other water masses in the ocean interior, maintaining CO_2 in the deep ocean[70,71]. Our reconstructed temporal changes in the latitudinal position of the ACC shows a generally linear relationship with atmospheric CO_2[72] (Fig. 5b). There is more scatter in the data of MIS 2-4 (towards bottom left in Fig. 5b), which may be due to effects of increased iron-fertilization in the SAZ on atmospheric CO_2 during these intervals that may not strictly correspond with ACC latitude change[5,12].

Two discrepancies between our reconstructed frontal latitude and the atmospheric CO_2 record are worth noting. Specifically, the fronts shifted strongly northward at MIS 5d while CO_2 declined only modestly, and the fronts shifted northward through the late Holocene while CO_2 rose (Figs. 4a, d and 5b). These discrepancies can be explained by the intensity of AZ upwelling (as reconstructed with diatom-bound $\delta^{15}N$[12]; Fig. 4g), which does not have a unique relationship with the mean latitude of the westerly winds. As previously discussed, the low obliquity at MIS 5d and the declining obliquity during the late Holocene should have increased the temperature gradient between the middle and high latitudes, which is supported by the increase in temperature difference between moisture source and ice core site of Vostok[73]. This increase in temperature gradient should have intensified the SWW, compensating for the equatorward displacement of the winds so as to maintain and/or increase upwelling and thus permit CO_2 outgassing from the AZ[12]. The progression of CO_2 level compared with that of ACC latitude during MIS 5d and the late Holocene with low(ering) obliquity falls towards the left of the linear trend, in contrast to MIS 5b with high obliquity that closely follows the linear trend (Fig. 5b), suggesting less CO_2 drawdown than predicted based on ACC latitude change, supporting a compensation from intensified SWW and strengthened upwelling. In addition, as described above, the strong SWW-driven (Ekman) transport of AZ surface waters northward driven by low(ering) obliquity at MIS 5d and the late Holocene may have worked to push surface isotherms northward (Fig. 5a). Together, these processes can explain the otherwise anomalous conditions of MIS 5d and the late Holocene of a northward frontal position (Fig. 4d), stronger AZ upwelling than expected from ACC latitude (Fig. 4g), and relatively high atmospheric CO_2 (Fig. 4a, b).

Two potential issues with this mechanism are noted here. First, the compiled data (Fig. 4) suggest that the role of obliquity on AZ upwelling was muted during the coldest climates of the last glacial cycle, as there is no evident deviation in the progression of Antarctic temperature or atmospheric CO_2 compared to ACC latitude during a cooling event at the end of MIS 3 when obliquity was low (Fig. 5). This may be due to greater sensitivity of AZ upwelling to changes in obliquity-driven SWW intensity when the SWW is more poleward. Another issue points to the stronger deviation during the late Holocene compared to MIS 5d, despite relatively higher obliquity of the former. In other words, the diatom-bound N isotope upwelling proxy and atmospheric CO_2 suggest that the enhancement of wind strength during the late Holocene was able to overcome the impact of northward ACC latitude to drive a trend of stronger AZ upwelling. Why? It is possible that the effect of obliquity on the strength of the SWW and subsequent effects on AZ upwelling and CO_2 outgassing is dependent on some other yet unclear climate components, which might arise in future studies by comparing similar low-obliquity intervals in several glacial-interglacial cycles.

Enabled by the application of the same paleothermometry method across a large latitudinal difference in the Southern Ocean and a framework imitating the impact of ACC migrations on Southern Ocean SST, the approach taken here provides a quantitative, temporally continuous view of how the boundary between the thermally contrasting Antarctic and subtropical surface waters has migrated over a full glacial cycle in the Indian Southern Ocean. The results suggest that cooling was a dominant driver of the equatorward shift of the SWW during the ice ages, with changes in the wind strength driven by obliquity also contributing to reconstructed changes. Through its effects on Southern Ocean upwelling and related vertical circulation, the equatorward shift of the SWW during ice ages should have enhanced the storage of carbon in the deep ocean, helping to explain the lower atmospheric CO_2 levels of the ice ages. During MIS 5d and the late Holocene, low obliquity and thus an increased mid-to-high latitude temperature gradient may have strengthened the westerly wind-driven AZ upwelling, compensating for the equatorward SWW location so as to sustain the upwelling in the AZ and thus maintaining/raising atmospheric CO_2[12]. At the same time, strong Ekman upwelling forces the ACC northward during these particular time intervals. Thus, the effects of obliquity may explain the deviation of MIS 5d and the late Holocene from the overarching tendency for a more northward ACC to be associated with Antarctic cooling, reduced AZ upwelling, and lower atmospheric CO_2 over the last glacial cycle.

The quantitative framework employed in this study is a rather coarse representation of the surface ocean temperature transition across the ACC and has multiple underlying assumptions. However, this approach is diagnostic and allows us to identify a robust connection between ACC latitude and climate in the Indian Southern Ocean, and to investigate its influence on atmospheric CO_2. With generation of SST records of higher resolution and refinements in the parameterization of the quantitative framework, this approach promises to provide multiple constraints on the climatic controls on ACC frontal location and circulation in different sectors of the Southern Ocean.

Methods

Study area. Marine sediment cores MD11-3353 (50.57°S, 68.39°E, 1568 m water depth) and MD11-3357 (44.68°S, 80.43°E, 3349 m water depth) were recovered by the *R.V. Marion Dufresne* in 2011 around the Kerguelen Archipelago in the southeast Indian Ocean (Fig. 1). Both cores were recently described elsewhere[12,41,62]. MD11-3353 is located slightly south of the modern Antarctic Polar Front (APF), whereas MD11-3357 is located in the Subantarctic Zone (SAZ), north of the Subantarctic Front (SAF). The Kerguelen Plateau exerts a strong influence on the ACC flow such that 60% of the current is deflected northwards of the Plateau, followed by a southeastward flow east of the plateau, and the integrated ACC flow is estimated to reach 150 Sv around the Kerguelen Plateau[74].

Age models. This study relies on previously published age models for all cores[12,41]. Briefly, the age model for MD11-3357 relies on graphical alignment of the GDGT-based SST reconstruction with the EDC deuterium record[41]. The original age model for MD11-3353[41], aligning GDGT-based SST with the EDC deuterium record, has been updated by adjusting the youngest and oldest tie points and adding two tie points in MIS 3 based on diatom-bound $\delta^{15}N$ correlation with the diatom-bound $\delta^{15}N$ record of MD12-3394[12].

SST reconstructions. GDGT measurements were performed at the Max Planck Institute for Chemistry (MPIC) following the method proposed in ref. [75]. Briefly, the GDGT-fraction was extracted from 3–5 g of freeze-dried sediment and simultaneously separated from other organic biomarkers using an Accelerated Solvent Extractor (ASE 350) and analyzed with a high-pressure liquid chromatograph coupled to a single quadrupole mass spectrometer detector (HPLC-MS; Agilent 1260 Infinity)[76]. Temperature of the surface ocean was reconstructed using a revised TEX^L_{86} calibration that linearly fits the global core-top TEX^L_{86}[42] to World Ocean Atlas 2009[45] 0–200 m integrated surface ocean temperature (Supplementary Note 1). Intra-laboratory standard TEX^L_{86}-SST error for replicate measurements of a standard sediment sample extracted in each batch of samples ($n = 13$) was 0.34 °C, similar to literature estimates[44]. We discuss the uncertainties in absolute SST reconstruction and ΔSST reconstruction by the updated calibration function in the Supplementary Note 3. We discuss potential contribution of non-thermal factors to the estimated TEX^L_{86} temperatures in the Kerguelen region over the last glacial-interglacial cycle using a series of GDGT-based indices in the Supplementary Note 5. We provide an estimate of the uncertainty of the reconstructed ΔSST in Supplementary Note 6.

ΔSST calculation. To calculate past ΔSST, the data from different cores have been interpolated at a time grid of 2.5 kyr, which best resembles the initial resolution in both cores. ΔSST was then determined by subtraction:

$$\Delta SST(t_x) = SST(t_x)_{core1} - SST(t_x)_{core2} \tag{1}$$

with t_x describing the same age point in the cores, core 1 being MD11-3357 and core 2 being MD11-3353.

Quantitative framework setup. The initial meridional SST profile is the zonally averaged annual mean temperature of 0–200 m depth of the region 68.5°E to 80.5°E, 34.5°S to 60.5°S from World Ocean Atlas 2009[45]. The initial meridional SST profile is simplified to three segments: the Antarctic Zone (AZ) segment, the Polar Transition Zone (PTZ, i.e., the Polar Frontal Zone (PFZ) and the SAZ combined) segment, and the Subtropical Zone (STZ) segment (Supplementary Fig. 15). From higher to lower latitudes, the AZ-PTZ boundary (denoted lat1) and PTZ-STZ boundary (denoted lat2) are the latitudes with the largest increase and decrease in the slope of the meridional SST profile, respectively. These changes in slope represent the transition from the cold polar surface water mass towards the warm STZ surface water. The SST within each segment was then fitted to a linear line:

$$SST_{AZ}(lat) = k_{AZ} * lat + m_{AZ}, lat < lat1 \tag{2}$$

$$SST_{PTZ}(lat) = k_{PTZ} * lat + m_{PTZ}, lat1 < lat < lat2 \tag{3}$$

$$SST_{STZ}(lat) = k_{STZ} * lat + m_{STZ}, lat > lat2 \tag{4}$$

Two parameters, $range_{AZ}$ and $range_{STZ}$, represent the maximum glacial-interglacial SST change (i.e., warmest SST minus coldest SST) in the two regions, respectively. EDC relative air temperatures were used as a reflection of Antarctic climate change. Temperature changes at EDC were transferred into different amounts of SST change in the AZ and the STZ due to polar amplification. For any given EDC temperature change at time *t*, we assume that the SST of the AZ and STZ will increase/decrease a fraction of the maximum SST change of the zone, and we can get the SST lines in the AZ and the STZ at time *t* (Supplementary Fig. 15, with the constraint that the lowest SST is −2 °C, the freezing point of sea water, for the AZ):

$$SST_{AZ}(t, lat)_{no\,shift} = k_{AZ} * lat + m_{AZ} + \frac{\Delta T_{EDC}(t)}{\max(\Delta T_{EDC}) - \min(\Delta T_{EDC})} * range_{AZ}, \quad lat < lat1 \tag{5}$$

$$SST_{STZ}(t, lat)_{no\,shift} = k_{STZ} * lat + m_{STZ} + \frac{\Delta T_{EDC}(t)}{\max(\Delta T_{EDC}) - \min(\Delta T_{EDC})} * range_{STZ}, \quad lat > lat2 \tag{6}$$

The new SST line of the PTZ segment at time *t* is a linear regression between the new SSTs at lat1 and lat2. (Supplementary

Fig. 15):

$$SST_{PTZ}(t, lat)_{no\,shift} = \frac{SST_{STZ}(t, lat2)_{no\,shift} - SST_{AZ}(t, lat1)_{no\,shift}}{lat2 - lat1} * lat + m'_{PTZ},\quad lat1 < lat < lat2 \tag{7}$$

We then assume that a change in Antarctic temperature leads to a latitudinal shift of all three SST lines, and the amount of shift is linearly related to the amount of EDC temperature change (note that the slopes of all three SST lines are the same as in the no-shift scenario):

$$\Delta lat(t) = a * \Delta T_{EDC}(t) + b(\Delta lat > 0 \text{ represents a poleward shift}) \tag{8}$$

The SST lines after the shift are:

$$SST_{AZ}(t, lat)_{shift} = k_{AZ} * (lat + \Delta lat(t)) + m_{AZ} + \frac{\Delta T_{EDC}(t)}{\max(\Delta T_{EDC}) - \min(\Delta T_{EDC})} * range_{AZ},\quad lat + \Delta lat(t) < lat1 + \Delta lat(t) \tag{9}$$

$$SST_{STZ}(t, lat)_{shift} = k_{STZ} * (lat + \Delta lat(t)) + m_{STZ} + \frac{\Delta T_{EDC}(t)}{\max(\Delta T_{EDC}) - \min(\Delta T_{EDC})} * range_{STZ},\quad lat + \Delta lat(t) > lat2 + \Delta lat(t) \tag{10}$$

$$SST_{PTZ}(t, lat)_{shift} = \frac{SST_{STZ}(t, lat2)_{no\,shift} - SST_{AZ}(t, lat1)_{no\,shift}}{lat2 - lat1} * (lat + \Delta lat(t)) + m'_{PTZ},\quad lat1 + \Delta lat(t) < (lat + \Delta lat(t)) < lat2 + \Delta lat(t) \tag{11}$$

Determination of the optimal parameters. To tune our model to match the reconstructed ΔSST, we need to determine the four variables: the maximum range of SST change in the AZ and STZ, i.e., $range_{AZ}$ and $range_{STZ}$, and the slope and intercept of the linear model between Δlat and ΔT_{EDC}, i.e., a and b. The sensitivity analysis (Supplementary Note 8) shows that $range_{AZ}$ and $range_{STZ}$ have limited impact on when the maximum ΔSST occurs, thus we tentatively choose 6 °C to be $range_{AZ}$ and 2.5 °C to be $range_{STZ}$, based on glacial temperature reconstructions[77].

The sensitivity analysis shows that with realistic values for *a*, the maximum ΔSST between the two sites would occur when the ACC is ~2° southward of its current position within the observed maximum ΔSST range (Supplementary Fig. 17). The maximum TEX^L_{86}-reconstructed ΔSST occurs when the temperature change at EDC is around −3 °C to −5 °C, and the sensitivity analysis shows that this only agrees with conditions of $b > 0$ (Supplementary Fig. 17), which means that the ACC should be southward of its current position when EDC temperature is at the current level, inconsistent with the frontal locations inferred from the modern meridional SST profile. This inconsistency leads us to consider the possibility that the modern ACC latitude is an outlier compared to the relationship between frontal movement and EDC temperature from MIS 6 to MIS 2 and we should consider a new initial meridional SST profile.

A straight-forward option is to choose the scenario when the steep PTZ segment is optimally sandwiched in between the core's locations as the new initial meridional SST profile. This would also be the scenario when ΔSST is the largest. According to the TEX^L_{86}-reconstructed data, this scenario would be when the temperature change at EDC is around −4 °C and the ACC is around 2° southward of its current position. However, the exact meridional SST profile of this time is unknown. According to the TEX^L_{86}-reconstructed data, when the EDC temperature change was between −3 °C and −5 °C, the frontal shift placed the steep PTZ segment between MD11-3353 and MD11-3357, and the mean value of the ΔSST is ~7.7 °C, which is similar to the SST difference between the two endpoints of the PFZ segment in the current WOA meridional SST profile, which is ~8 °C. Thus, it is a fair estimate that the new initial scenario is the current meridional SST profile shifted 2° southward, at the time when the EDC temperature change was −4 °C. The actual meridional SST profile may be higher or lower than our assumed profile, but for the ΔSST, the difference in the absolute value will be canceled off. We define Δlat′ as the ACC latitude relative to the new initial SST profile, and the relationship between Δlat and ΔT_{EDC} becomes:

$$\Delta lat' = \Delta lat - 2 = a' * \Delta T'_{EDC} + b' = a' * [\Delta T_{EDC} - (-4)] + b' \tag{12}$$

We take $range_{AZ} = 6$ °C, and $range_{STZ} = 2.5$°C and use sequential least squares programming (SLSQP) optimizer to find a' within [0, +inf] and b' within [−inf, +inf] that best fit the reconstructed data. The resulting a' and b' with realistic values that produce the smallest difference between the modeled results and the actual data is 0.58 and −0.12, respectively (Supplementary Fig. 19):

$$\begin{aligned} \Delta lat' &= \Delta lat - 2 = a' * \Delta T'_{EDC} + b' = a' * [\Delta T_{EDC} - (-4)] + b' \\ \Delta lat - 2 &= 0.58 * \Delta T'_{EDC} - 0.12 = 0.58 * [\Delta T_{EDC} - (-4)] - 0.12 \\ \Delta lat &= 0.58 * \Delta T_{EDC} + 4.20 \end{aligned} \tag{13}$$

With this best-fitting pair of a' and b', the ACC shifts southward(northward) by ~0.58° with every °C of EDC warming(cooling). When EDC temperature change is 0 relative to the modern ($\Delta T_{EDC} = 0$), the ACC is 4.20° south of its current position (Δlat = 4.20).

Reconstruction of ACC latitude changes in the past 150 kyr. Based on the relationship between the ΔSST of sites MD11-3357 and MD11-3353 and the change of ACC latitude inferred from our framework, we use the reconstructed TEX^L_{86}-SST at the two sites to reconstruct the relative frontal positions of the past 150 kyr. Because the relationship is non-monotonic, within the relevant range, each ΔSST corresponds to two ACC positions, and we select the position that makes more sense for the corresponding EDC temperature in our optimized model: If the EDC temperature is lower than −4 °C, we choose the latitude that is more southward than 2° (the upper part of the curve in Supplementary Fig. 21). When ΔSST is higher than 6.7 °C and lower than 7.7 °C, the lower limit of the confidence interval for reconstructed ACC that is more southward than 2° (i.e., the upper part of the curve) is assumed to deviate the same amount from the reconstructed ACC latitude as the upper limit, and the upper limit of the confidence interval for the lower part of the curve is assumed to deviate the same amount from the reconstructed ACC latitude as the lower limit. When ΔSST is higher than 7.7 °C, the reconstructed ACC latitude is taken to be the mean of the upper and lower limit and is represented by the dashed line in Fig. 4d.

Data availability

The TEX^L_{86}-SST records calculated with the original calibration for 0–200 m integrated temperature[33] are available from the PANGAEA database: https://doi.pangaea.de/10.1594/PANGAEA.931020 and https://doi.pangaea.de/10.1594/PANGAEA.907123. The biomarker fractional abundances and indices and TEX^L_{86}-SST calculated with the revised calibration for each core site, the SST gradient between the two sites, and the reconstructed Antarctic Circumpolar Current latitude change in the last 150 kyr are available from the Zenodo data repository (https://doi.org/10.5281/zenodo.10479199).

Code availability

MATLAB and Python code used for data analysis and quantitative framework simulations are available from the corresponding author upon request.

Received: 6 July 2023; Accepted: 11 January 2024;
Published online: 30 January 2024

References

1. Burke, A. & Robinson, L. F. The Southern Ocean's role in carbon exchange during the last deglaciation. *Science* **335**, 557–561 (2012).
2. Skinner, L. C., Fallon, S., Waelbroeck, C., Michel, E. & Barker, S. Ventilation of the deep Southern Ocean and deglacial CO_2 rise. *Science* **328**, 1147–1151 (2010).
3. Keeling, R. F. & Stephens, B. B. Antarctic sea ice and the control of Pleistocene climate instability. *Paleoceanography* **16**, 112–131 (2001).
4. Martin, J. H. & Glacial-interglacial, C. O. 2 change: the iron hypothesis. *Paleoceanography* **5**, 1–13 (1990).
5. Martínez-García, A. et al. Iron fertilization of the Subantarctic Ocean during the last ice age. *Science* **343**, 1347–1350 (2014).
6. François, R. et al. Contribution of Southern Ocean surface-water stratification to low atmospheric CO_2 concentrations during the last glacial period. *Nature* **389**, 929–935 (1997).
7. Watson, A. J. & Naveira Garabato, A. C. The role of Southern Ocean mixing and upwelling in glacial-interglacial atmospheric CO_2 change. *Tellus B: Chem. Phys. Meteorol.* **58**, 73–87 (2006).
8. Watson, A. J., Vallis, G. K. & Nikurashin, M. Southern Ocean buoyancy forcing of ocean ventilation and glacial atmospheric CO_2. *Nat. Geosci.* **8**, 861–864 (2015).
9. Sigman, D. M. et al. The Southern Ocean during the ice ages: a review of the Antarctic surface isolation hypothesis, with comparison to the North Pacific. *Quat. Sci. Rev.* **254**, 106732 (2021).
10. Studer, A. S. et al. Antarctic Zone nutrient conditions during the last two glacial cycles. *Paleoceanography* **30**, 845–862 (2015).
11. Wang, X. T. et al. Deep-sea coral evidence for lower Southern Ocean surface nitrate concentrations during the last ice age. *Proc. Natl Acad. Sci. USA* **114**, 3352–3357 (2017).
12. Ai, X. E. et al. Southern Ocean upwelling, Earth's obliquity, and glacial-interglacial atmospheric CO_2 change. *Science* **370**, 1348–1352 (2020).
13. Toggweiler, J. R., Russell, J. L. & Carson, S. R. Midlatitude westerlies, atmospheric CO_2, and climate change during the ice ages. *Paleoceanography* **21**, n/a-n/a (2006).
14. Anderson, R. F. et al. Wind-driven upwelling in the Southern Ocean and the deglacial rise in atmospheric CO_2. *Science* **323**, 1443–1448 (2009).
15. Toggweiler, J. R. & Russell, J. Ocean circulation in a warming climate. *Nature* **451**, 286–288 (2008).
16. Marshall, J. & Speer, K. Closure of the meridional overturning circulation through Southern Ocean upwelling. *Nat. Geosci.* **5**, 171–180 (2012).
17. Dong, S., Sprintall, J. & Gille, S. T. Location of the Antarctic polar front from AMSR-E satellite sea surface temperature measurements. *J. Phys. Oceanogr.* **36**, 2075–2089 (2006).
18. Orsi, A. H., Whitworth, T. & Nowlin, W. D. On the meridional extent and fronts of the Antarctic Circumpolar Current. *Deep Sea Res. Part I: Oceanogr. Res. Pap.* **42**, 641–673 (1995).
19. Sigman, D. M. & Boyle, E. A. Glacial/interglacial variations in atmospheric carbon dioxide. *Nature* **407**, 859–869 (2000).
20. Sokolov, S. & Rintoul, S. R. Circumpolar structure and distribution of the Antarctic Circumpolar Current fronts: 1. Mean circumpolar paths. *J. Geophys. Res. Oceans* **144**, C11018 (2009).
21. Böning, C. W., Dispert, A., Visbeck, M., Rintoul, S. R. & Schwarzkopf, F. U. The response of the Antarctic Circumpolar Current to recent climate change. *Nat. Geosci.* **1**, 864–869 (2008).
22. Saenko, O. A., Fyfe, J. C. & England, M. H. On the response of the oceanic wind-driven circulation to atmospheric CO_2 increase. *Clim. Dyn.* **25**, 415–426 (2005).
23. Graham, R. M., de Boer, A. M., Heywood, K. J., Chapman, M. R. & Stevens, D. P. Southern Ocean fronts: controlled by wind or topography? *J. Geophys. Res. Oceans* **117**, C08018 (2012).
24. Nair, A. et al. Southern Ocean sea ice and frontal changes during the Late Quaternary and their linkages to Asian summer monsoon. *Quat. Sci. Rev.* **213**, 93–104 (2019).
25. Civel-Mazens, M. et al. Antarctic Polar Front migrations in the Kerguelen Plateau region, Southern Ocean, over the past 360 kyrs. *Glob. Planet. Change* **202**, 103526 (2021).
26. Gersonde, R., Crosta, X., Abelmann, A. & Armand, L. Sea-surface temperature and sea ice distribution of the Southern Ocean at the EPILOG Last Glacial Maximum—a circum-Antarctic view based on siliceous microfossil records. *Quat. Sci. Rev.* **24**, 869–896 (2005).
27. Brathauer, U. & Abelmann, A. Late Quaternary variations in sea surface temperatures and their relationship to orbital forcing recorded in the Southern Ocean (Atlantic sector). *Paleoceanography* **14**, 135–148 (1999).
28. Sikes, E. L. et al. Southern Ocean seasonal temperature and Subtropical Front movement on the South Tasman Rise in the late Quaternary. *Paleoceanography* **24**, PA2201 (2009).
29. Bard, E. & Rickaby, R. E. M. Migration of the subtropical front as a modulator of glacial climate. *Nature* **460**, 380–383 (2009).
30. Kohfeld, K. E. et al. Southern Hemisphere westerly wind changes during the Last Glacial Maximum: paleo-data synthesis. *Quat. Sci. Rev.* **68**, 76–95 (2013).
31. Schouten, S., Hopmans, E. C., Schefuß, E. & Sinninghe Damsté, J. S. Distributional variations in marine crenarchaeotal membrane lipids: a new tool for reconstructing ancient sea water temperatures? *Earth Planet. Sci. Lett.* **204**, 265–274 (2002).
32. Kim, J.-H. et al. Holocene subsurface temperature variability in the eastern Antarctic continental margin. *Geophys. Res. Lett.* **39**, L06705 (2012).
33. Kim, J.-H. et al. New indices and calibrations derived from the distribution of crenarchaeal isoprenoid tetraether lipids: Implications for past sea surface temperature reconstructions. *Geochim. Cosmochim. Acta* **74**, 4639–4654 (2010).
34. Fogwill, C. J., Turney, C. S. M., Hutchinson, D. K., Taschetto, A. S. & England, M. H. Obliquity control on southern hemisphere climate during the last glacial. *Sci. Rep.* **5**, 11673 (2015).
35. Uemura, R. et al. Asynchrony between Antarctic temperature and CO_2 associated with obliquity over the past 720,000 years. *Nat. Commun.* **9**, 961 (2018).
36. Studer, A. S. et al. Enhanced stratification and seasonality in the Subarctic Pacific upon Northern Hemisphere Glaciation—new evidence from diatom-bound nitrogen isotopes, alkenones and archaeal tetraethers. *Earth Planet. Sci. Lett.* **351–352**, 84–94 (2012).
37. Hayes, C. T. et al. A stagnation event in the deep South Atlantic during the last interglacial period. *Science* **346**, 1514–1517 (2014).
38. Levy, R. et al. Antarctic ice sheet sensitivity to atmospheric CO_2 variations in the early to mid-Miocene. *Proc. Natl Acad. Sci. USA* **113**, 3453–3458 (2016).
39. Sangiorgi, F. et al. Southern Ocean warming and Wilkes Land ice sheet retreat during the mid-Miocene. *Nat. Commun.* **9**, 317 (2018).
40. Etourneau, J. et al. Ocean temperature impact on ice shelf extent in the eastern Antarctic Peninsula. *Nat. Commun.* **10**, 304 (2019).
41. Thöle, L. M. et al. Glacial-interglacial dust and export production records from the Southern Indian Ocean. *Earth Planet. Sci. Lett.* **525**, 115716 (2019).
42. Tierney, J. E. & Tingley, M. P. A TEX86 surface sediment database and extended Bayesian calibration. *Sci. Data* **2**, 150029 (2015).
43. Inglis, G. N. & Tierney, J. E. *The TEX86 Paleotemperature Proxy* (Cambridge University Press, 2020).
44. Schouten, S. et al. An interlaboratory study of TEX86 and BIT analysis of sediments, extracts, and standard mixtures. *Geochem. Geophys. Geosyst.* **14**, 5263–5285 (2013).
45. Locarnini, R. et al. *World Ocean Atlas 2009, Vol. 1: Temperature*. Vol. 68, 184 (2010).
46. Shevenell, A. E., Ingalls, A. E., Domack, E. W. & Kelly, C. Holocene Southern Ocean surface temperature variability west of the Antarctic Peninsula. *Nature* **470**, 250–254 (2011).
47. Kaiser, J., Schefuß, E., Lamy, F., Mohtadi, M. & Hebbeln, D. Glacial to Holocene changes in sea surface temperature and coastal vegetation in north central Chile: high versus low latitude forcing. *Quat. Sci. Rev.* **27**, 2064–2075 (2008).
48. Jouzel, J. et al. Orbital and millennial Antarctic climate variability over the past 800,000 years. *Science* **317**, 793–796 (2007).
49. Pichon, J.-J. et al. Surface water temperature changes in the high latitudes of the southern hemisphere over the Last Glacial-Interglacial Cycle. *Paleoceanography* **7**, 289–318 (1992).
50. Labeyrie, L. et al. Hydrographic changes of the Southern Ocean (southeast Indian Sector) Over the last 230 kyr. *Paleoceanography* **11**, 57–76 (1996).
51. Schneider, T., O'Gorman, P. A. & Levine, X. J. Water vapor and the dynamics of climate changes. *Rev. Geophys.* **48**, RG3001 (2010).
52. Kohfeld, K. E. & Chase, Z. Temporal evolution of mechanisms controlling ocean carbon uptake during the last glacial cycle. *Earth Planet. Sci. Lett.* **472**, 206–215 (2017).
53. O'Neill, L. W., Chelton, D. B. & Esbensen, S. K. Observations of SST-induced perturbations of the wind stress field over the Southern Ocean on seasonal timescales. *J. Clim.* **16**, 2340–2354 (2003).
54. Moore, J. K., Abbott, M. R. & Richman, J. G. Location and dynamics of the Antarctic Polar Front from satellite sea surface temperature data. *J. Geophys. Res.* **104**, 3059–3073 (1999).
55. Sallée, J. B., Speer, K. & Morrow, R. Response of the Antarctic circumpolar current to atmospheric variability. *J. Clim.* **21**, 3020–3039 (2008).
56. Sokolov, S. & Rintoul, S. R. Circumpolar structure and distribution of the Antarctic Circumpolar Current fronts: 2. Variability and relationship to sea surface height. *J. Geophys. Res. Oceans* **114**, C11019 (2009).
57. Pauthenet, E. et al. Seasonal meandering of the polar front upstream of the Kerguelen Plateau. *Geophys. Res. Lett.* **45**, 9774–9781 (2018).

58. Marcott, S. A., Shakun, J. D., Clark, P. U. & Mix, A. C. A reconstruction of regional and global temperature for the past 11,300 years. *Science* **339**, 1198–1201 (2013).
59. Zielinski, U., Gersonde, R., Sieger, R. & Fütterer, D. Quaternary surface water temperature estimations: Calibration of a diatom transfer function for the Southern Ocean. *Paleoceanography* **13**, 365–383 (1998).
60. Lu, J., Chen, G. & Frierson, D. M. W. The position of the midlatitude storm track and eddy-driven westerlies in aquaplanet AGCMs. *J. Atmos. Sci.* **67**, 3984–4000 (2010).
61. Timmermann, A. et al. Modeling obliquity and CO_2 effects on Southern Hemisphere climate during the past 408 ka. *J. Clim.* **27**, 1863–1875 (2014).
62. Studer, A. S. et al. Increased nutrient supply to the Southern Ocean during the Holocene and its implications for the pre-industrial atmospheric CO2 rise. *Nat. Geosci.* **11**, 756–760 (2018).
63. Jones, D. C., Ito, T. & Lovenduski, N. S. The transient response of the Southern Ocean pycnocline to changing atmospheric winds. *Geophys. Res. Lett.* **38**, L15604 (2011).
64. Lamy, F. et al. Precession modulation of the South Pacific westerly wind belt over the past million years. *Proc. Natl Acad. Sci. USA* **116**, 23455–23460 (2019).
65. Frierson, D. M. W., Lu, J. & Chen, G. Width of the Hadley cell in simple and comprehensive general circulation models. *Geophys. Res. Lett.* **34**, L18804 (2007).
66. Shakun, J. D., Lea, D. W., Lisiecki, L. E. & Raymo, M. E. An 800-kyr record of global surface ocean $\delta^{18}O$ and implications for ice volume-temperature coupling. *Earth Planet. Sci. Lett.* **426**, 58–68 (2015).
67. Lee, S.-Y. & Poulsen, C. J. Obliquity and precessional forcing of continental snow fall and melt: implications for orbital forcing of Pleistocene ice ages. *Quat. Sci. Rev.* **28**, 2663–2674 (2009).
68. Brayshaw, D. J., Hoskins, B. & Blackburn, M. The storm-track response to idealized SST perturbations in an aquaplanet GCM. *J. Atmos. Sci.* **65**, 2842–2860 (2008).
69. Ferrari, R. et al. Antarctic sea ice control on ocean circulation in present and glacial climates. *PNAS* **111**, 8753–8758 (2014).
70. Lund, D. C., Adkins, J. F. & Ferrari, R. Abyssal Atlantic circulation during the Last Glacial Maximum: constraining the ratio between transport and vertical mixing. *Paleoceanography* **26**, PA1213 (2011).
71. De Boer, A. M. & Hogg, A. McC. Control of the glacial carbon budget by topographically induced mixing. *Geophys. Res. Lett.* **41**, 4277–4284 (2014).
72. Bereiter, B. et al. Revision of the EPICA Dome C CO_2 record from 800 to 600 kyr before present: analytical bias in the EDC CO_2 record. *Geophys. Res. Lett.* **42**, 542–549 (2015).
73. Vimeux, F., Cuffey, K. M. & Jouzel, J. New insights into Southern Hemisphere temperature changes from Vostok ice cores using deuterium excess correction. *Earth Planet. Sci. Lett.* **203**, 829–843 (2002).
74. Park, Y.-H. et al. Polar Front around the Kerguelen Islands: an up-to-date determination and associated circulation of surface/subsurface waters. *J. Geophys. Res.: Oceans* **119**, 6575–6592 (2014).
75. Auderset, A., Schmitt, M. & Martínez-García, A. Simultaneous extraction and chromatographic separation of n-alkanes and alkenones from glycerol dialkyl glycerol tetraethers via selective Accelerated Solvent Extraction. *Org. Geochem.* **143**, 103979 (2020).
76. Hopmans, E. C., Schouten, S. & Sinninghe Damsté, J. S. The effect of improved chromatography on GDGT-based palaeoproxies. *Org. Geochem.* **93**, 1–6 (2016).
77. Waelbroeck, C. et al. Constraints on the magnitude and patterns of ocean cooling at the Last Glacial Maximum. *Nat. Geosci.* **2**, 127–132 (2009).
78. Hersbach, H. et al. The ERA5 global reanalysis. *Q. J. R. Meteorol. Soc.* **146**, 1999–2049 (2020).
79. Bell, B. et al. The ERA5 global reanalysis: Preliminary extension to 1950. *Q. J. R. Meteorol. Soc.* **147**, 4186–4227 (2021).
80. GEBCO Bathymetric Compilation Group 2021. The GEBCO_2021 Grid—a continuous terrain model of the global oceans and land. https://doi.org/10.5285/C6612CBE-50B3-0CFF-E053-6C86ABC09F8F (2021).
81. Berger, A. & Loutre, M. F. Insolation values for the climate of the last 10 million years. *Quat. Sci. Rev.* **10**, 297–317 (1991).

Acknowledgements
We gratefully thank H. Eri Amsler, Julia Gottschalk, Thomas Frölicher, Gianna Battaglia, Fortunat Joos and Xavier Crosta for fruitful discussions. We thank Bichen Zhang for help with setting up the quantitative framework. Financial support for this study was provided by the Swiss National Science Foundation (grants P1BEP2_168625 to L.M.T. and PP00P2_144811 and PP00P2_172915 to S.L.J.), the Max Planck Society (A.M.G.), the ERC starting GRANT OceaNice (grant 802835 to P.K.B.), and the U.S. National Science Foundation (grant PLR-1401489 to D.M.S.).

Author contributions
L.M.T., X.E.A., S.L.J., A.M.G., and D.M.S. devised the study. L.M.T., A.A., S.M., and M.S. performed the GDGT analyses supervised by A.M.G. L.M.T. calculated the SST difference between the two sites. X.E.A. set up the quantitative framework and ran simulations. E.M. and A.M. planned the cruise to retrieve the sediment cores presented here. A.S.S., M.W., and P.K.B. contributed to data interpretation. X.E.A. and L.M.T. wrote the manuscript with editing by D.M.S. and contributions from all co-authors.

Funding
Open Access funding enabled and organized by Projekt DEAL.

Competing interests
The authors declare no competing interests.

Additional information
Supplementary information The online version contains supplementary material available at https://doi.org/10.1038/s43247-024-01216-x.

Correspondence and requests for materials should be addressed to Xuyuan E. Ai, Lena M. Thöle, Alfredo Martínez-García or Samuel L. Jaccard.

Peer review information *Communications Earth & Environment* thanks Matthew Chadwick, Shuzhuang Wu and the other, anonymous, reviewer(s) for their contribution to the peer review of this work. Primary Handling Editors: Aliénor Lavergne. A peer review file is available.